

NASA/TM-2013-217966



# Evaluation of Delamination Onset and Growth Characterization Methods under Mode I Fatigue Loading

*Gretchen B. Murri*

*Langley Research Center, Hampton, Virginia*

---

February 2013

## NASA STI Program . . . in Profile

Since its founding, NASA has been dedicated to the advancement of aeronautics and space science. The NASA scientific and technical information (STI) program plays a key part in helping NASA maintain this important role.

The NASA STI program operates under the auspices of the Agency Chief Information Officer. It collects, organizes, provides for archiving, and disseminates NASA's STI. The NASA STI program provides access to the NASA Aeronautics and Space Database and its public interface, the NASA Technical Report Server, thus providing one of the largest collections of aeronautical and space science STI in the world. Results are published in both non-NASA channels and by NASA in the NASA STI Report Series, which includes the following report types:

- **TECHNICAL PUBLICATION.** Reports of completed research or a major significant phase of research that present the results of NASA Programs and include extensive data or theoretical analysis. Includes compilations of significant scientific and technical data and information deemed to be of continuing reference value. NASA counterpart of peer-reviewed formal professional papers, but having less stringent limitations on manuscript length and extent of graphic presentations.
- **TECHNICAL MEMORANDUM.** Scientific and technical findings that are preliminary or of specialized interest, e.g., quick release reports, working papers, and bibliographies that contain minimal annotation. Does not contain extensive analysis.
- **CONTRACTOR REPORT.** Scientific and technical findings by NASA-sponsored contractors and grantees.

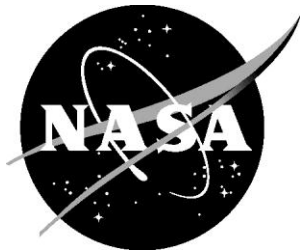
- **CONFERENCE PUBLICATION.** Collected papers from scientific and technical conferences, symposia, seminars, or other meetings sponsored or co-sponsored by NASA.
- **SPECIAL PUBLICATION.** Scientific, technical, or historical information from NASA programs, projects, and missions, often concerned with subjects having substantial public interest.
- **TECHNICAL TRANSLATION.** English-language translations of foreign scientific and technical material pertinent to NASA's mission.

Specialized services also include organizing and publishing research results, distributing specialized research announcements and feeds, providing information desk and personal search support, and enabling data exchange services.

For more information about the NASA STI program, see the following:

- Access the NASA STI program home page at <http://www.sti.nasa.gov>
- E-mail your question to [help@sti.nasa.gov](mailto:help@sti.nasa.gov)
- Fax your question to the NASA STI Information Desk at 443-757-5803
- Phone the NASA STI Information Desk at 443-757-5802
- Write to:  
STI Information Desk  
NASA Center for AeroSpace Information  
7115 Standard Drive  
Hanover, MD 21076-1320

NASA/TM-2013-217966



# Evaluation of Delamination Onset and Growth Characterization Methods under Mode I Fatigue Loading

*Gretchen B. Murri*  
*Langley Research Center, Hampton, Virginia*

National Aeronautics and  
Space Administration

Langley Research Center  
Hampton, Virginia 23681-2199

---

February 2013

Trade names and trademarks are used in this report for identification only. Their usage does not constitute an official endorsement, either expressed or implied, by the National Aeronautics and Space Administration.

Available from:

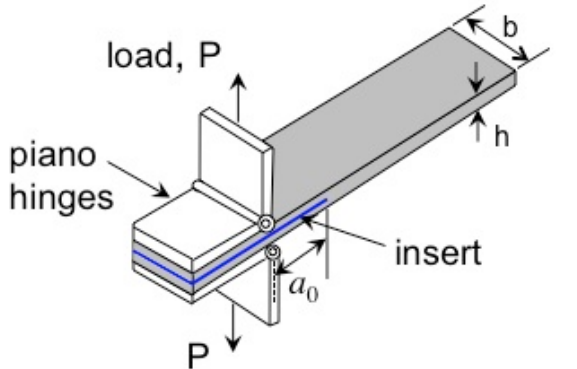
NASA Center for AeroSpace Information  
7115 Standard Drive  
Hanover, MD 21076-1320  
443-757-5802

## Abstract

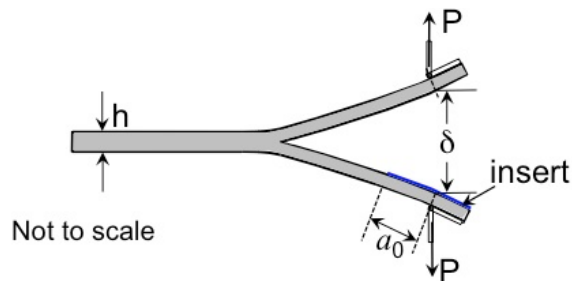
Reliable delamination characterization data for laminated composites are needed for input to analytical models of structures to predict delamination onset and growth. The double-cantilevered beam (DCB) specimen is used to measure fracture toughness,  $G_{Ic}$ , and strain energy release rate,  $G_{I\max}$ , for delamination onset and growth under cyclic loading in laminated composites. In the current study, DCB specimens of IM7/8552 graphite/epoxy supplied by two different manufacturers were tested in static and fatigue to compare the experimentally measured characterization data from the two sources, and to evaluate the usefulness of a proposed ASTM standard for generating Paris Law type equations for delamination growth, including the effects of fiber bridging. Both the modified beam theory (MBT) and modified compliance calibration (MCC) methods were used to calculate  $G_I$  values. Static results were used to generate compliance calibration constants for reducing the fatigue data, and a delamination resistance curve,  $G_{IR}$ , for each material, which was used to determine the effects of fiber-bridging on the delamination growth data. Specimens were tested in fatigue at an initial cyclic  $G_{I\max}$  level equal to 50, 40 or 30% of the fracture toughness,  $G_{Ic}$ , to determine a delamination onset curve and the delamination growth rate. The delamination onset curve equations had similar exponents and the same trends, however one source had consistently longer lifetimes to delamination onset. Delamination growth rate was calculated by plotting  $da/dN$  versus  $G_{I\max}$  on a log-log scale and fitting a Paris Law to the data. Two different data reduction methods, a 2-point and a 7-point fit, were used to calculate  $da/dN$  and the resulting Paris Law equations were compared. To determine the effects of fiber-bridging, growth rate results were normalized by the delamination resistance curve for each material and compared to the non-normalized results. Paris Law exponents were found to decrease by 31% to 37% due to normalizing the growth data. Normalizing the data also greatly reduced the amount of scatter between the different specimens. Visual data records from the fatigue testing were also used to calculate individual compliance calibration constants from the fatigue data for some of the specimens. The resulting  $da/dN$  versus  $G_{I\max}$  plots showed much improved repeatability between specimens of each source compared to using averaged values from the static data. The Paris Law expressions for the two sources also showed the closest agreement using the individually fit compliance data.

## Introduction

The most common failure mechanism in laminated composite materials is delamination damage. In order to optimize the use of fiber-reinforced composite materials in primary aircraft structures, damage tolerance under static and fatigue loading must be thoroughly understood. Reliable delamination characterization data for laminated composites are needed to use as input in analytical models of structures to predict delamination onset and growth. The double-cantilevered beam (DCB) specimen, shown in Fig. 1, is used to measure mode I fracture toughness,  $G_{Ic}$ , and strain energy release rate,  $G_{I\max}$ , for delamination onset and growth in laminated composites under mode I fatigue loading. Reference 1 is a standardized test method for measuring static fracture toughness,  $G_{Ic}$ , using the DCB specimen. Reference 2 is a standardized test method for determining the onset of delamination and a threshold level,  $G_{I\text{th}}$ , below which delamination will not start in fatigue. However, there is currently no standard for determining the delamination growth rate in fatigue, after delamination begins. Reference 3 is a proposed test standard for delamination growth in Mode I specimens under constant amplitude fatigue loading and is currently being studied by means of a testing Round Robin through ASTM Committee D30.



(a) Isometric view



(b) Side view showing opening displacement,  $\delta$

Figure 1. Double-cantilevered beam (DCB) specimen. Figures are not to scale.

For composite materials, delamination growth has typically been related to the cyclic strain energy release rate,  $G$ . In ref. 4 and 5, delamination growth onset data from edge-delamination (EDT) and end-notched flexure (ENF) tests were used to generate threshold curves, below which delamination would not initiate. A minimum threshold for no-delamination-growth was assumed to exist at a loading level for which there was no delamination growth at 1 million cycles.

Delamination growth in a constant-amplitude displacement-controlled DCB test yields decreasing  $G_{\text{Imax}}$  values. Therefore, delamination growth from onset to arrest can be considered to have 3 phases, as shown in Fig. 2: a region of rapid growth at high (but sub-critical) values of  $G$ , a linear growth region, and a slow growth region where the delamination approaches an arrest point, or apparent threshold, below which delamination will not grow. A full-fatigue characterization equation of the form shown on Fig. 2 has been proposed [4-7] to express the complete delamination growth behavior in terms of the maximum cyclic  $G$ -value,  $G_{\text{Imax}}$ ; the threshold value at delamination arrest,  $G_{\text{Ith}}$ ; and the static fracture toughness,  $G_c$ . The equation of the linear portion of this curve is known as the Paris Law,  $da/dN=A(G_{\text{Imax}})^B$ , and is typically used to characterize stable delamination growth.

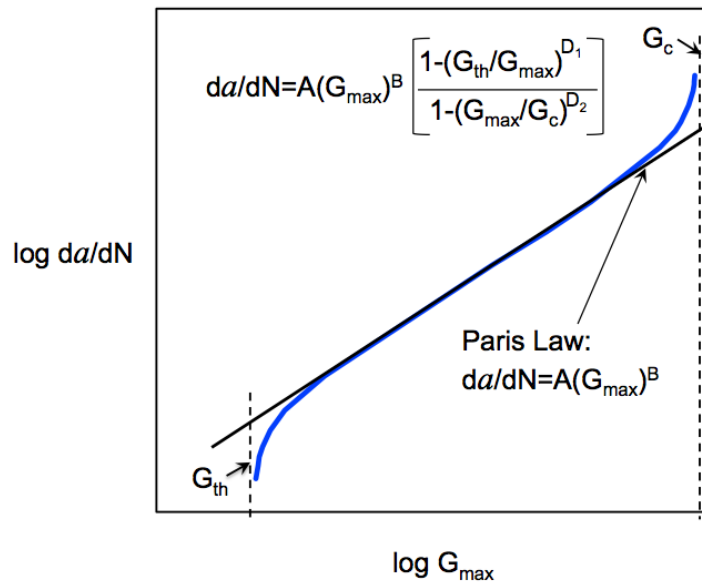


Figure 2. Full-fatigue delamination characterization plot.

Because the DCB specimen is unidirectional, some nesting of fibers between adjacent plies can occur, resulting in fiber-bridging at the delaminating interface. As a delamination grows, the fiber-bridging acts to resist the delamination, causing an artificial increase in the measured toughness [5-9], which will affect the resulting Paris Law. However, this fiber-bridging is not a material property, but an artifact of the unidirectional specimen. In actual structures, delaminations typically grow between plies of dissimilar orientation and fiber-bridging does not occur. Therefore, in order to be useful in structural modeling, expressions relating the delamination growth rate and strain energy release rate must be corrected for the

effect of fiber-bridging. Fiber-bridging under quasi-static loading can be quantified as a delamination resistance ( $G_{IR}$ ) curve, which can be used to correct the growth data for the fiber-bridging effects [6-7, 9-11].

In this study, DCB specimens of IM7/8552 graphite/epoxy were tested under Mode I static and fatigue loading to determine delamination characterization properties. Specimens were provided from two different manufacturers. The IM7/8552 prepreg materials were provided to them and the panels were made according to their own internal specifications, and hence may have slight differences. The objectives of the study were to generate static and fatigue delamination data necessary for finite element (FE) modeling of IM7/8552 composite sub-element models, and to compare the static and fatigue results from the two different sources to assess the effect of differences in the same material due to variations in end user specifications on characterization data. A similar comparison was made for the mode II response of IM7/8552 from the same two sources in ref. 12. An additional objective of this study was to evaluate the usefulness of the proposed ASTM standard for generating Paris Law type expressions for delamination growth, including the effects of fiber bridging.

Quasi-static tests were conducted first, to determine the fracture toughness, delamination resistance curve, and test parameters and compliance constants for fatigue loading. Fatigue tests were then conducted at initial  $G_{I\max}$  levels of 50, 40, or 30% of  $G_{Ic}$ , to determine fatigue delamination onset behavior and growth rates, which were expressed in the form of a Paris law. Both a 2-point secant method and a 7-point sliding-fit method were used to reduce the delamination growth data and the resulting Paris Law fits were compared. The delamination resistance equations were used to normalize the growth data to account for the effects of fiber-bridging. A Paris Law fit was applied to both the non-normalized and normalized data sets and the results were compared.

Reference 1 specifies that the modified beam theory (MBT) and modified compliance calibration (MCC) data reduction methods are both acceptable for calculating strain energy release rate,  $G_I$ ; however MBT is the recommended method because it tends to yield the most conservative values [1]. The specimens used in these tests not only were produced by two different manufacturers, but were also cut from different panels, and consequently had variations in thickness and initial delamination length. Because only the MCC calculation is a function of the specimen thickness, both the MBT and MCC data reduction methods were used to reduce the data, and the results were compared, to determine the effect of differences in specimen geometry on calculated  $G_{I\max}$ . The effect of variations in the compliance calibration constants on the Paris Law was also evaluated. Initially, the compliance calibration constants used to reduce the fatigue data were calculated from averaged static data, in accordance with refs. 2 and 3. For approximately half of the specimens, compliance constants were also generated for each specimen separately, using visual data from the fatigue tests, and the  $G_I$  results were recalculated and the Paris Law expressions were compared.

## Materials And Specimens

Specimens of IM7/8552 graphite/epoxy were tested under static and fatigue loading. Specimens were provided from two different suppliers (Source 1 and

Source 2), who manufactured the panels and cut them into specimens. The 24-ply, 0° unidirectional specimens were nominally 1-inch (25.4mm) wide and 7-inch (178mm) long. All specimens were manufactured with a thin Teflon film at the mid-plane at one end to simulate an initial delamination. The Teflon insert was 0.0005 inch (13 $\mu$ m) thick and nominally 3.0 inch (76.2mm) long.

Prior to testing, specimens were dried using the procedure in ASTM D5229 [13]. After drying, the width and thickness of each specimen were measured to the nearest 0.001mm, using a micrometer, at the center and each end. The average specimen width,  $b$ , was 0.9989 inch (25.37mm) for Source 1 and 0.9973 inch (25.33mm) for Source 2. The average specimen thickness,  $h$ , was 0.1771 inch (4.50mm) for both sources. However, specimen thicknesses from different panels varied from 0.1720 inch (4.37mm) to 0.185 inch (4.70mm) for Source 1 and from 0.1681 inch (4.27mm) to 0.192 inch (4.88mm) for Source 2.

Load was applied to the specimens through piano hinges, which were bonded to the specimens using a 2-part epoxy adhesive, which was cured at 300°F for 1 hour. After the specimens cooled, they were stored in a desiccator until testing. A schematic of the DCB specimen is shown in Fig. 1, with the piano hinges, thickness ( $h$ ), width ( $b$ ), and initial delamination ( $a_0$ ) indicated. The initial delamination length,  $a_0$ , is the distance from the load-point line to the interior end of the insert, and was nominally 2.0 inch (50.8mm). The opening displacement,  $\delta$ , is measured at the application point, as shown in Fig. 1(b). Immediately before testing, the edges of the specimen were coated with a thin layer of white paint and marked in 1mm increments, starting from the tip of the insert to a length of 60mm.

## Experimental Procedures

All tests were conducted under displacement control in a small table-top servo-hydraulic test stand using a 100-lb load cell. A photograph of the specimen and test fixture is shown in Fig. 3. The tests were controlled by a computer program, which also recorded the test output data. For all of the static specimens, and approximately half of the fatigue specimens of each source, a 2-Megapixel digital camera was used to monitor the delamination growth and the image was displayed on a computer monitor. Tests were conducted under room temperature conditions. After completing each test, the specimen was split apart at the mid-plane so that the initial and final delamination lengths could be more accurately determined, and to verify that the delamination grew evenly across the specimen width.

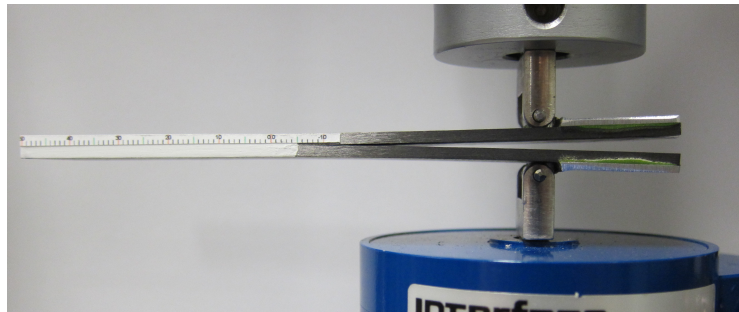


Figure 3. Double-cantilevered beam specimen and loading fixture.

## Static Tests

Quasi-static tests were performed on four specimens from each source to determine the fracture toughness,  $G_{Ic}$ . The static tests were also used to determine compliance calibration constants for fatigue data reduction and the delamination resistance curves,  $G_{IR}$ . Static tests were conducted according to ASTM Standard D5528 [1]. Displacement was applied at a rate of 0.02 in/min (0.508 mm/min). The computer program recorded load, displacement, and compliance every 0.1 seconds. The camera system recorded a photograph of the specimen edge every 0.5 seconds, along with the corresponding applied displacement and load. Opening displacement,  $\delta$ , was applied to the specimen until delamination growth initiated and then was continued until the delamination had grown to at least the 40mm marker. Visual recordings of the delamination length along the specimen edge were also made at every 1mm of growth for the first 10 mm, and then at every 5 mm of growth for the remainder of the test. Figure 4 shows an example of a typical load-displacement curve from a static test, with the critical point and visual delamination recordings indicated.

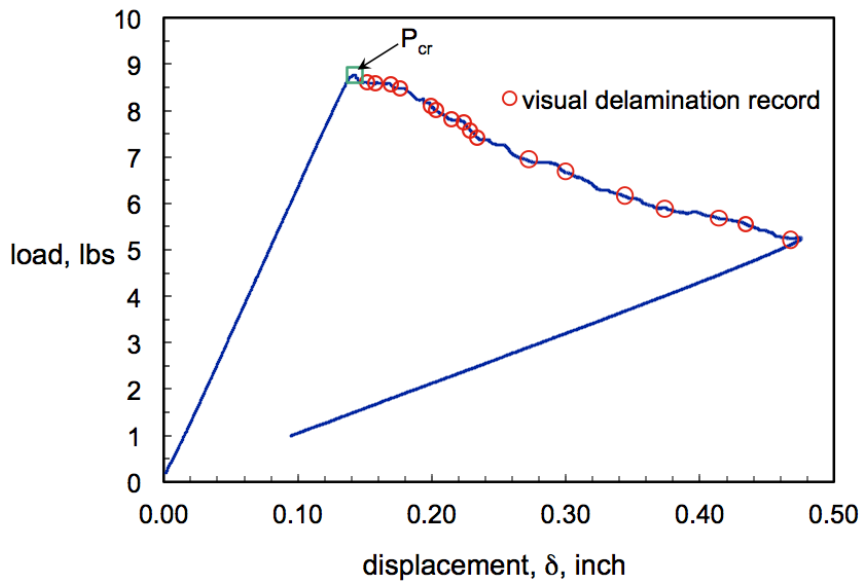


Figure 4. Load-displacement plot for static DCB specimen.

## Fatigue Tests for Delamination Onset Threshold

To generate a delamination onset threshold curve, specimens were tested in fatigue, using the procedures described in ASTM Standard D6115 [2]. Tests were conducted under displacement control, at a frequency of 5 cycles/second. The ratio of minimum displacement to maximum displacement (R-ratio) was  $\delta_{min}/\delta_{max} = 0.1$ . Prior to fatigue testing, each specimen was loaded quasi-statically, to a maximum displacement that was less than the mean cyclic displacement for that test. This was done in order to determine the initial specimen compliance, and to help verify

the location of the insert tip. Specimens of each source were tested at a range of initial cyclic  $G_{I\max}$  levels chosen as a percentage of the average  $G_{Ic}$  from the static tests. For each desired  $G_{I\max}$  level ( $X\%G_{Ic}$ ), the maximum cyclic displacement ( $\delta_{\max}$ ) for testing was determined from the relationship

$$G_{I\max} = X\%G_{Ic} = \frac{3\delta_{\max}^2}{2b(a+|\Delta|)} \times \frac{1}{C} \quad (1)$$

where  $C$  is the initial specimen compliance,  $b$  is the specimen width,  $a$  is the initial delamination length, and  $|\Delta|$  is a compliance constant determined from the static testing.

During the fatigue testing, the computer system recorded maximum and minimum loads ( $P$ ), maximum and minimum displacements ( $\delta$ ), compliance ( $C$ ), and cycle count ( $N$ ), at every 10 cycles. The camera system recorded a photograph of the specimen edge at every 1000 cycles, taking the photo at the point of maximum cyclic displacement. A computer file was generated which enabled the photo number to be related to the number of loading cycles at which it occurred.

### Fatigue Tests for Delamination Growth Rate

In addition to delamination onset data, fatigue tests were used to generate delamination growth rate data, according to the specifications of the draft standard [3]. The test apparatus, specimen preparation, and procedures required by ref. 3 are identical to those of standard D6115 [2] for delamination growth onset. Therefore, each fatigue test specimen was used to generate both delamination onset data and delamination growth data, by cycling to the onset point, and then continuing the fatigue cycling uninterrupted to generate growth data. Specimens were cycled until the delamination growth rate had decreased to at least  $1 \times 10^{-7}$  in/cycle ( $2.54 \times 10^{-6}$  mm/cycle), or until no growth had been detected by at least  $1.5 \times 10^6$  cycles.

## Results And Discussion

### Static Tests

#### *Compliance Coefficients And Fracture Toughness*

For both specimen sources, fracture toughness was calculated using the Modified Beam Theory (MBT) and Modified Compliance Calibration (MCC) methods, as described in ref. 1. For the MBT method,  $G_{Ic}$  is given by

$$G_{Ic} = \frac{3P\delta}{2b(a+|\Delta|)} \quad (2)$$

and for MCC,  $G_{Ic}$  is given by

$$G_{Ic} = \frac{3P^2 C^{2/3}}{2bA_1 h} \quad (3)$$

where  $P$  is the load,  $\delta$  is the displacement,  $b$  is the specimen width,  $a$  is the initial delamination length,  $C$  is the compliance, and  $h$  is the specimen thickness. The constants  $A_1$  and  $|\Delta|$  are compliance constants determined from the visually recorded delamination data from the static tests (as shown in Fig. 4).

For the MBT method, the relationship between the specimen compliance and delamination length is

$$C^{1/3} = m(a + |\Delta|) \quad (4)$$

The constants  $m$  and  $|\Delta|$  are determined by a least squares line fit to a plot of the observed delamination lengths ( $a$ ) from the static test versus the cube root of the corresponding compliance ( $C$ ). For each source, the combined  $a$  vs.  $C^{1/3}$  data for all the static specimens were plotted together to determine  $m$  and  $|\Delta|$  values to use in the data reduction. Figure 5 shows the static data and resulting compliance parameters for Source 2, where each different symbol on the figure represents a different static specimen.

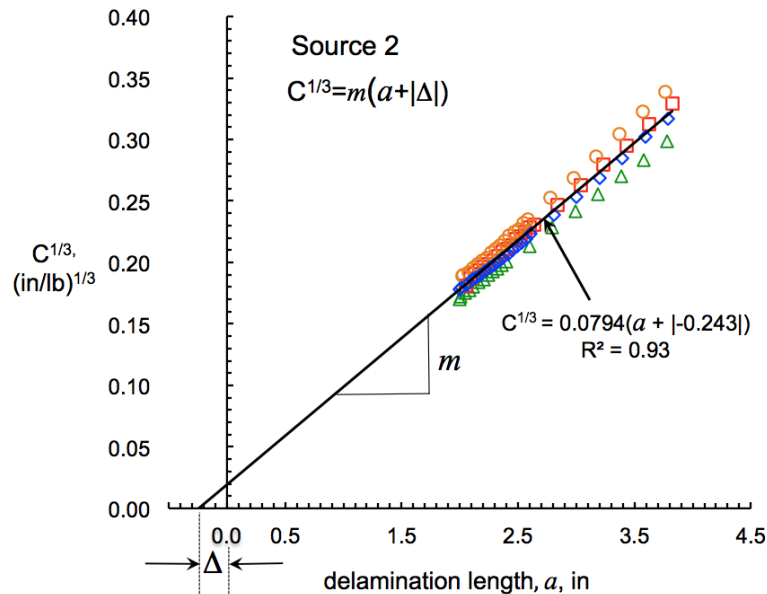


Figure 5. Compliance calibration fit to static data for MBT.

A similar method was used to determine the compliance constants for the MCC data reduction method. In this case, the relationship between the specimen compliance and delamination length is found from a least squares plot of the

delamination length normalized by specimen thickness ( $a/h$ ) versus the cube root of the corresponding compliance:

$$\frac{a}{h} = A_1 * C^{1/3} + k \quad (5)$$

Figure 6 shows the resulting compliance constants for Source 2 for the MCC method.

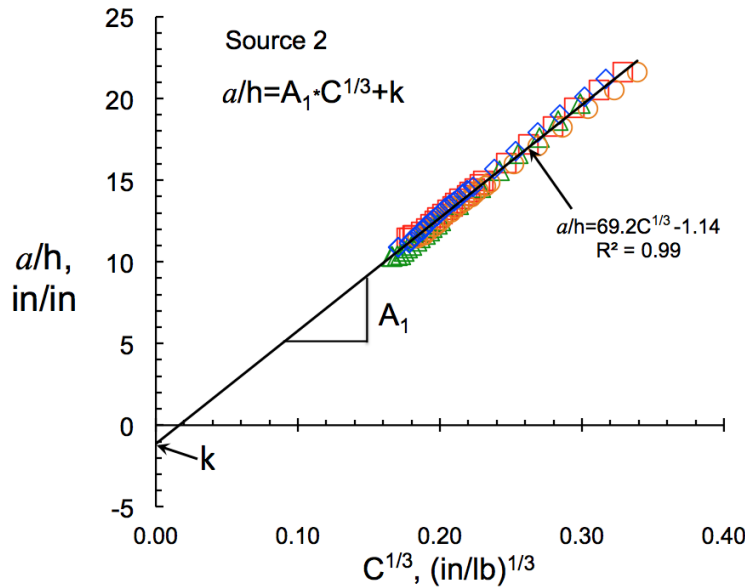


Figure 6. Compliance calibration fit to static data for MCC.

Comparing Figs. 5 and 6 shows that there is less scatter in the MCC results and a slightly higher Coefficient of Determination ( $R^2$ ). This may be because the MCC data uses  $a/h$  (rather than  $a$ ) and therefore is not affected by the large thickness variation that was observed in specimens cut from different panels. Similar results were observed for the Source 1 static tests. Fracture toughness values for both sources were initially calculated using both data reduction methods to determine whether one method was preferred for these specimens.

The compliance calibration coefficients for both the MBT and MCC methods, as well as the static  $G_{Ic}$  results for Source 1 and Source 2 are shown in Table 1. The compliance calibration coefficients for both methods were very similar for the two specimen sources. Both the MBT and MCC methods gave an average  $G_{Ic}$  value of 1.37 in-lb/in<sup>2</sup> (239.9 J/m<sup>2</sup>) for the Source 1 specimens. Average  $G_{Ic}$  values for Source 2 were approximately 13% higher than Source 1, at 1.55 in-lb/in<sup>2</sup> (271.4 J/m<sup>2</sup>) from MBT and 1.57 in-lb/in<sup>2</sup> (274.9 J/m<sup>2</sup>) from MCC. In ref. 12, static end-notched flexure tests were performed to determine the mode II fracture toughness,  $G_{IIc}$ , of precracked specimens of the identical source materials used here. Measured  $G_{IIc}$  values from Source 2 were approximately 9% higher than from Source 1.

Table 1. Static DCB Data

	MBT			MCC		
	$m_2$ (in/lb) $^{1/3}$ /in ((mm/N) $^{1/3}$ /mm)	$ \Delta $ , in (mm)	$G_{lc}$ , in-lb/in $^2$ (J/m $^2$ )	$A_1$ , (lb/in) $^{1/3}$ ((N/mm) $^{1/3}$ )	$k$ , in/in (mm/mm)	$G_{lc}$ , in-lb/in $^2$ (J/m $^2$ )
Source 1	0.0791 (0.00557)	0.259 (6.57)	1.37 (239.9)	68.8 (38.5)	-1.12	1.37 (239.9)
Source 2	0.0794 (0.00559)	0.243 (6.17)	1.55 (271.4)	69.2 (38.7)	-1.14	1.57 (274.9)

### *Delamination Resistance Curve*

In order to evaluate and correct for the effects of fiber-bridging in the fatigue data, the static test results were also used to determine a delamination resistance curve (R-curve) equation, for each source, to be used in the delamination growth data reduction. During the static testing, after the critical displacement point was reached, opening displacement was continued, and  $G_I$  was calculated at prescribed increments as the delamination continued to grow. The calculated  $G$ -values were plotted vs. the corresponding visually observed increase in delamination length ( $\Delta a$ ) to produce an R-curve for each source. Figure 7 shows an example of an R-curve for the Source 1 specimens, where the calculated MCC  $G$ -values are shown. The increasing  $G_I$  values suggest that there is some fiber-bridging occurring as delaminations grow in these specimens. As the figure shows, there was an increasing R-curve throughout the loading, with a constant slope for approximately the first 0.5-inch (12.7mm) of delamination growth, followed by another linear region, with a different slope, over the final 1.2 inches (30.5mm) of delamination growth. Because the delamination growth in the fatigue specimens never exceeded 0.5-inch, only the data points at  $\Delta a$  less than 0.5-inch were used to determine the  $G_{IR}$  equation. The  $G_{IR}$  equation was determined by fitting a least-squares curve to the combined static data from each source. The resulting  $G_{IR}$  equation, shown on Fig. 7, was used later to normalize the fatigue growth data. The  $G_{IR}$  equations for both sources are shown in Table 2.

Table 2. Delamination Resistance Curve ( $G_{IR}$ ) Equations

	$G_{IR}$ , in-lb/in $^2$
Source 1	$1.594 \Delta a + 1.22$ , $\Delta a \leq 0.5$ inch
Source 2	$1.337 \Delta a + 1.429$ , $\Delta a \leq 0.6$ inch

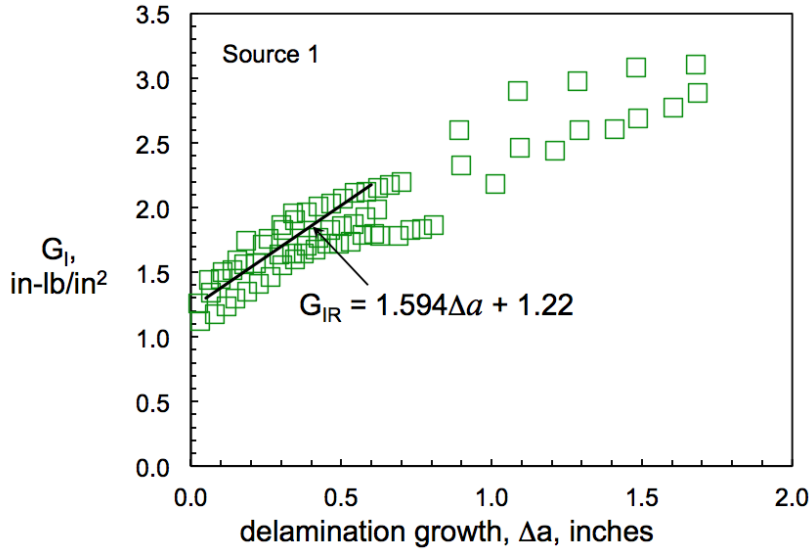


Figure 7. Delamination resistance curve from static DCB tests.

### Fatigue Tests for Delamination Onset Threshold

To produce a delamination threshold curve, specimens were tested in fatigue at target  $G_{I\max}$  levels equal to 50, 40, and 30% of the average  $G_{Ic}$  from the static tests. Under constant-amplitude displacement control in fatigue,  $G_{I\max}$  decreases from the initial value as the delamination grows. Therefore, the applied  $G_{I\max}$  listed for each test is the initial value. After the fatigue testing was completed on each specimen, the specimen was split along the midplane, and the initial delamination length was more accurately measured and the initial  $G_{I\max}$  was recalculated. Therefore, the actual initial  $G_{I\max}$  levels varied from 60% to 27%. A minimum of four specimens from each source was tested at target levels of 50, 40 and 30%  $G_{Ic}$ . Additionally, two specimens from Source 1 were tested at levels over 50% $G_{Ic}$ . To determine the threshold curve, the number of cycles corresponding to a decrease in the specimen compliance of 1% and 5% was recorded, as recommended in ref. 2.

Figure 8 shows the onset results for Source 1 using the MCC data reduction method. The average fracture toughness,  $G_{Ic}$ , is plotted at N=1. The three tests at the highest cycle counts are shown with right-pointing arrows, indicating that these are run-out tests, for which no delamination growth occurred. Results are generally in good agreement for tests at initial  $G_{I\max}$  of 50% $G_{Ic}$  or lower. The onset results for Source 2 are shown in Fig. 9, along with the average  $G_{Ic}$  value plotted at N=1. The right-pointing arrows indicate run-out tests. For this specimen set, the results are in reasonably good agreement for most of the data, however, there is noticeably more scatter in the results at the lowest load level.

Typically, a power curve is fit through the data sets, to give a  $G_{I\text{th}}$  threshold ( $G_{I\text{th}}$ ) below which delamination should not occur [4, 5]. The Kaleidagraph data plotting software [14] was used to find the best-fit power curve for both data sets, including the average  $G_{Ic}$  value but excluding the run-out results. The curve fit equations are shown on Figs. 8 and 9. Figure 10(a) shows the onset data and curves

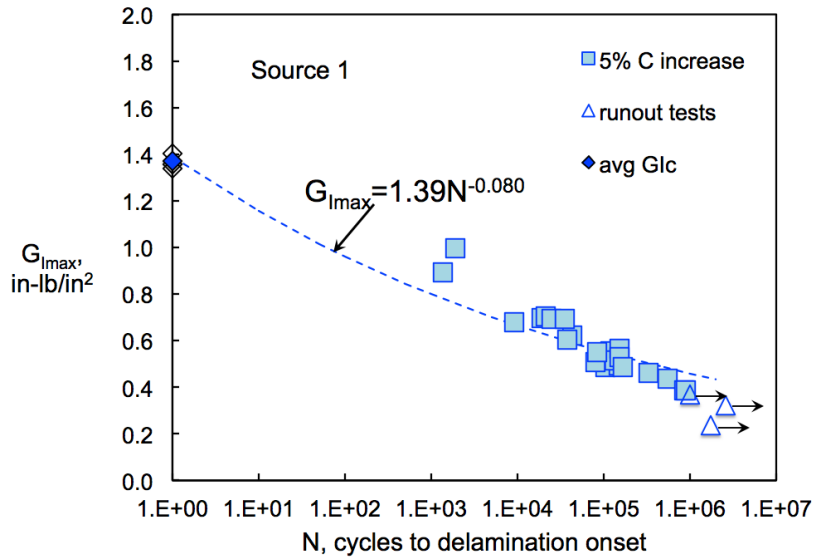


Figure 8. Delamination onset curve for Source 1.

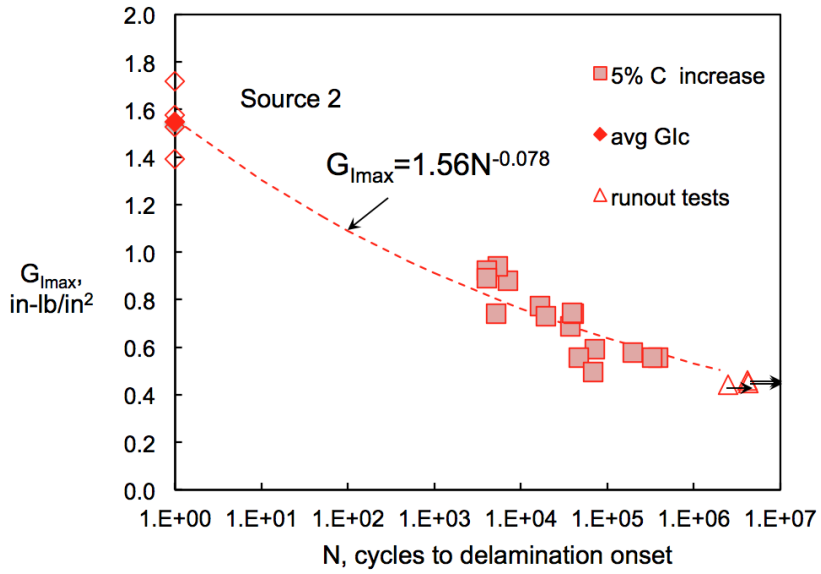
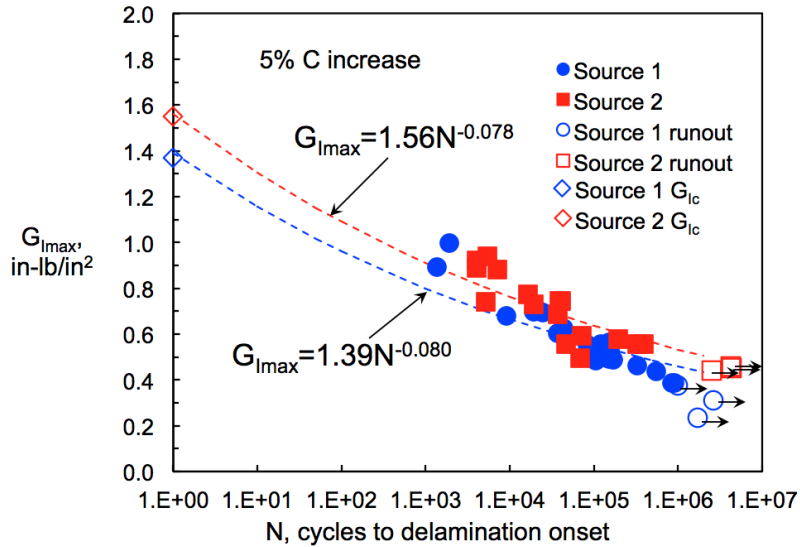
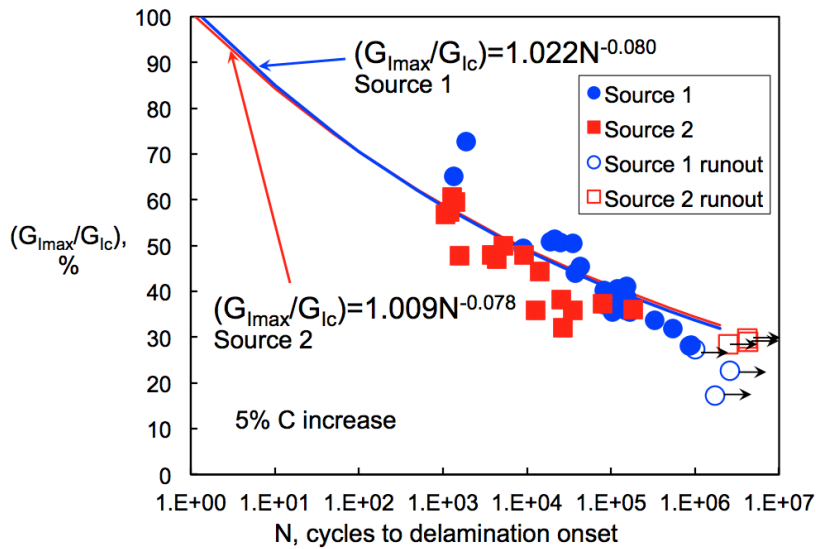


Figure 9. Delamination onset curve for Source 2.

for both sources. Although there is some overlap between the two source data sets, the number of cycles to onset is higher for the Source 2 specimens compared to Source 1, at comparable  $G_{lmax}$  values. Although the onset curves have similar exponents and the same trend, at low  $G_{lmax}$  levels the onset life of the Source 2 specimens is almost an order of magnitude greater than Source 1. Figure 10(b) shows the same data, with the  $G_{lmax}$  results expressed as the percentage of  $G_{lc}$  for each material. The onset curves are now almost identical and the equations in terms of  $G_{lmax}/G_{lc}$  are shown on the plot. In ref. 12, delamination onset curves were generated under mode II loading, using specimens from the same sources used in this study. Those curves were found to be nearly identical for the two sources.



(a) Onset life versus initial  $G_{I\max}$ .



(b) Onset life versus  $\%G_{Ic}$ .

Figure 10. Delamination onset curves for Sources 1 and 2.

### Fatigue Tests for Delamination Growth Rate

#### *Raw Data Parsing*

Fatigue growth data were generated using the same specimens used to generate the delamination onset data, by continuing the fatigue cycling beyond the onset point. Because the final raw data sets were very large, a parsing routine was first applied to the raw data to eliminate noise and reduce the data set to a more manageable size. This parsing routine compared the change in delamination length for each pair of consecutive data lines to a pre-set limit, and eliminated data points

for which the delamination length increase was less than this limit. Figure 11 shows an example of compliance vs. the number of loading cycles for the raw data set and for the parsed data set. The noise in the raw data set can make it difficult to determine trends in the reduced G data. Parsing removes most of the noise and therefore yields more useful reduced data. The parsed compliance data were used to calculate the delamination length at each data point, using equation (4) or (5), (MBT and MCC, respectively) along with the compliance fit constants from Table 1. The calculated  $a$  values, along with load and compliance from the parsed data, were used to generate the  $G_I$  and  $da/dN$  results for every specimen.

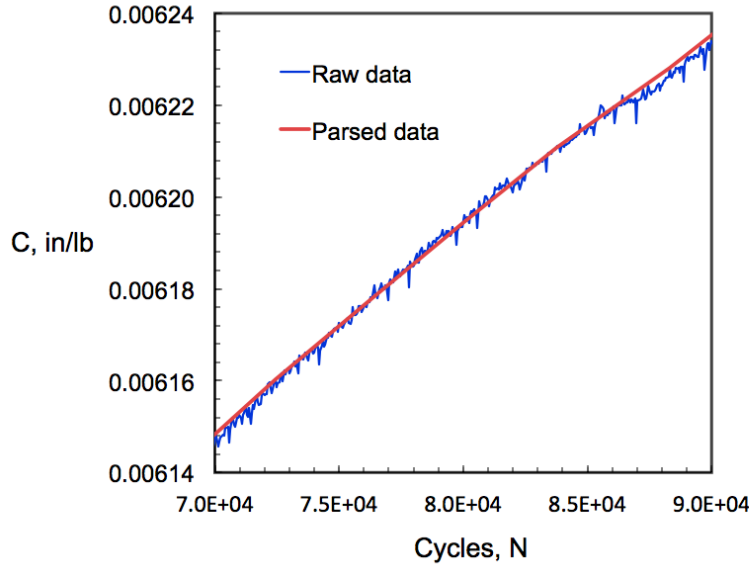


Figure 11. Compliance results for raw and parsed data sets.

### 2-point and 7-point $da/dN$ calculations

Reference 3 recommends two methods for determining the delamination growth rate,  $da/dN$ ; a 2-point secant method and a 7-point sliding-fit method. For the 2-point method,  $da/dN$  is determined from the slope of the line between two adjacent points on the plot of  $a$  (delamination length) vs.  $N$  (cycle count.) The corresponding value of  $G_{I\max}$  is calculated from either eq. (2) or (3), (MBT and MCC, respectively), where  $a$ ,  $P$ , and  $C$  are the averaged values from the two data points. The 7-point method calculates  $da/dN$  by fitting a second-order polynomial to each set of 7 successive data points. The polynomial is used to calculate the value of  $a$  at the midpoint of the 7-point data set. The corresponding  $G_{I\max}$  value is calculated from either eq. (2) or (3), where  $P$  and  $C$  are the average values over the interval. A complete description of this method can be found in ASTM Standard E647-00 [15].

Figure 12 shows the  $da/dN$  vs.  $G_{I\max}$  results from both the 2-point and 7-point  $da/dN$  calculation methods for a Source 2 specimen tested at 40% $G_{Ic}$ , along with

the Paris Law equations fit to each data set. The Paris Law expressions are very similar for the two methods, but the scatter in the data is much less for the 7-point fit method. These results were typical for all the specimens tested, with the exponent of the Paris Law equation differing by about 3% or less between the 2-point and 7-point methods. Therefore, the 7-point fit method was considered to accurately represent the delamination growth, with less scatter, and was used to calculate  $da/dN$  for all the tests.

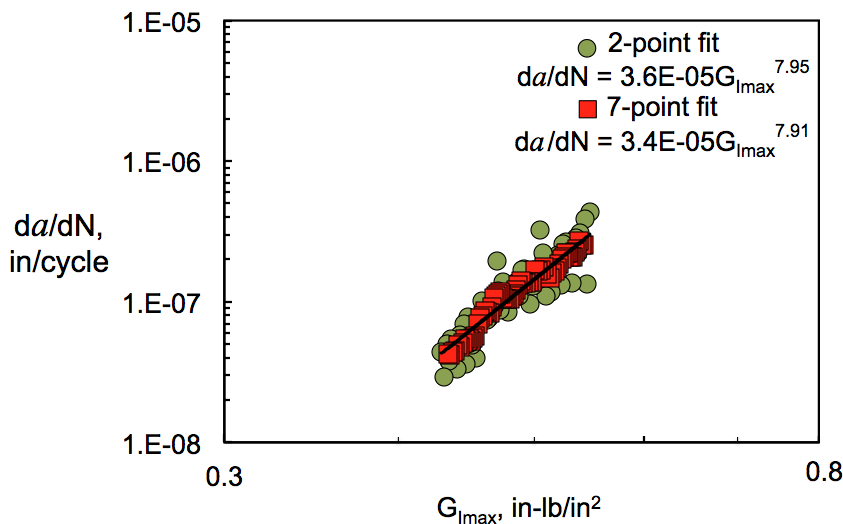


Figure 12. 2-point and 7-point data reduction comparison.

#### *MBT And MCC Data Reduction*

Plots of  $da/dN$  vs.  $G_{lmax}$  were generated for all the fatigue specimens from both sources, using both the MBT and MCC data reduction methods. Figures 13 and 14 show results for 23 specimens from Source 1, tested at  $G_{lmax}$  levels between 73% and 27%  $G_{lc}$ . The results are similar for the two  $G_{lmax}$  calculation methods. For both calculation methods, the slopes from the different specimens appear similar, but the position along  $G_{lmax}$  varies significantly, with a tendency for the data to shift to the left as the initial  $G_{lmax}$  value of the specimen decreases. Figures 15 and 16 show the  $da/dN$  vs.  $G_{lmax}$  results for 16 Source 2 specimens (MBT and MCC results, respectively.) Again, the data from the two methods are similar, although the MCC results are in a slightly more compact group. Like the Source 1 data, the Source 2 specimens seemed to have similar slopes, but different positions along  $G_{lmax}$ , although the data are less spread out than the Source 1 results. The scatter observed in Figs. 13-16 is likely due to differences in specimen geometry and varying amounts of fiber-bridging that occurred.

Because of the range of the data sets across  $G_{lmax}$ , fitting a Paris Law equation to the combined data resulted in a line that has a much flatter slope than any of the individual specimens and therefore did not reflect the behavior of any of the specimens. Therefore, a Paris Law equation was fit to each specimen separately and the constants and slopes were averaged for each data set. The resulting

equations for each method are shown on the figures. The Paris Law exponents are similar for all the plots, and are slightly lower using the MCC calculation for both sources. However, the constants, which reflect the position along the  $G_{I\max}$  axis, are very different, ranging from 0.001 for the Source 1 MBT results to 0.00005 for the Source 2 MCC results. This value affects the prediction of the delamination growth rate at the onset and at delamination arrest. The constant values shown are the averages of all the specimens in the set. Because of the spread of the data sets, these values are not very useful for generating a valid Paris Law.

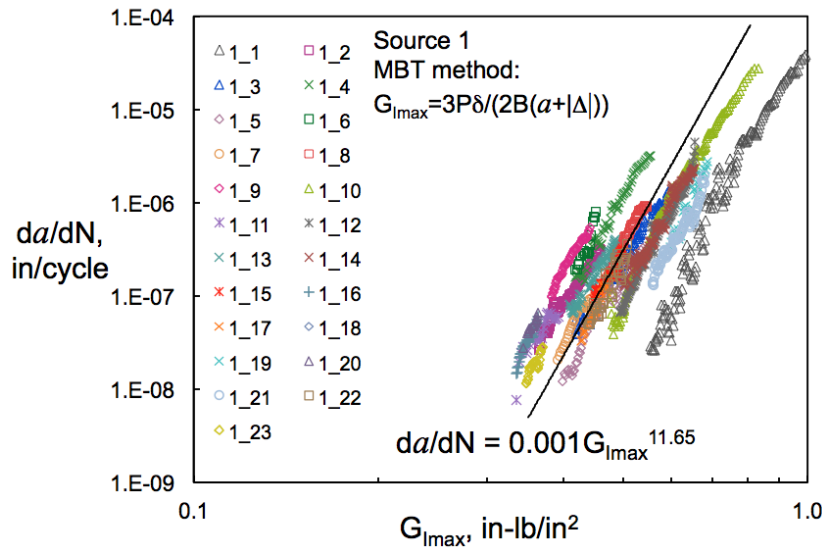


Figure 13. Delamination growth results for Source 1 using MBT. Paris Law equation is average of 23 individual specimens.

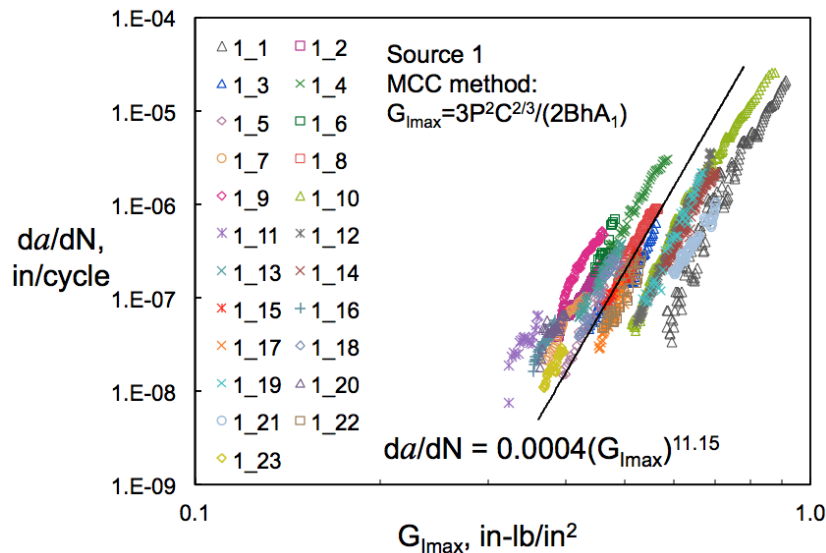


Figure 14. Delamination growth results for Source 1 using MCC. Paris Law equation is average of 23 individual specimens.

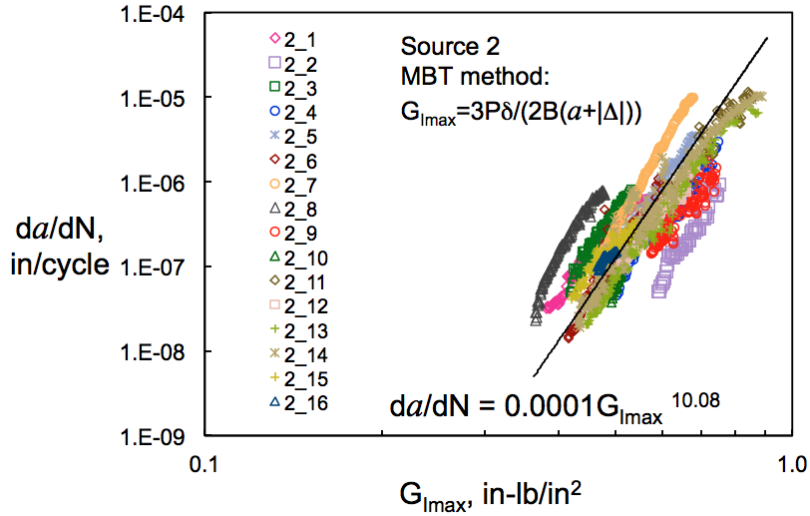


Figure 15. Delamination growth results for Source 2 using MBT. Paris Law equation is average of 16 individual specimens.

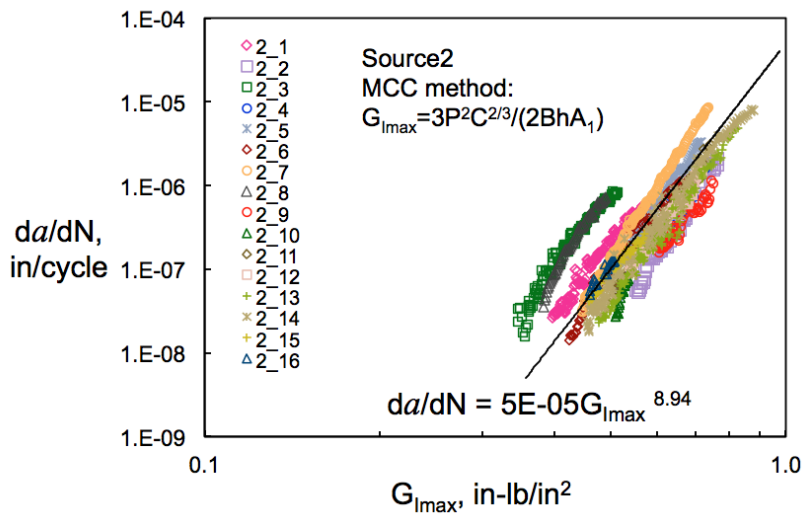


Figure 16. Delamination growth results for Source 2 using MCC. Paris Law equation is average of 16 individual specimens.

For both sources, using the MCC data reduction caused some specimens to noticeably shift position either to the right or left compared to the MBT solution. This occurred in specimens that were significantly thicker or thinner than the average. Although there was little difference between the combined results using the MBT or MCC data reduction method for either source material, the MCC method seemed to result in slightly more compact data sets (especially for Source 2) and therefore, the remainder of the results were calculated using MCC only.

### Normalized $G_{I\max}$ Results

Because the static specimens exhibited a rising R-curve, it is reasonable to assume that the fatigue data are also affected by fiber-bridging. Therefore, the  $G_{I\max}$  data were normalized by the delamination resistance curves and the data were replotted. At each data point, the  $G_{I\max}$  value was divided by  $G_{IR}$ , using the appropriate equation from Table 2. The normalized values,  $\bar{G}_{I\max}/G_{IR}$ , were then plotted versus  $da/dN$  and compared to the non-normalized results. In order to directly compare the unitless normalized results ( $\bar{G}_{I\max}/G_{IR}$ ) to the  $G_{I\max}$  results, the normalized results were multiplied by  $G_{lc}$ . This value was called  $\bar{G}_{I\max}$  and is plotted in Fig. 17 along with the non-normalized results for a Source 1 specimen, tested at  $G_{I\max}=37\%G_{lc}$ . A Paris Law equation has been fit to each data set. As the figure shows, the slope of the normalized results is not as steep and the exponent of the Paris Law is decreased by 35.8% from the non-normalized results. Figure 18 shows results for a Source 2 specimen tested at 59% $G_{lc}$ . For this case, normalizing the data reduced the exponent of the Paris Law by 29.5%. For all specimens tested, normalizing the  $G_{I\max}$  results resulted in a decrease in the Paris Law exponent of between 28.1% and 41.5%, compared to the non-normalized results. The average decrease was 37.1% for the Source 1 specimens and 31.5% for the Source 2 specimens. As Figs. 17 and 18 demonstrate, the effect of fiber-bridging on delamination growth rate can be significant, especially at high  $G_{I\max}$  levels. These results are consistent with the behavior observed in ref. 10 and 11, where it was shown that for a material with extensive fiber-bridging, the difference between the normalized and non-normalized delamination rate could quickly become an order of magnitude or more.

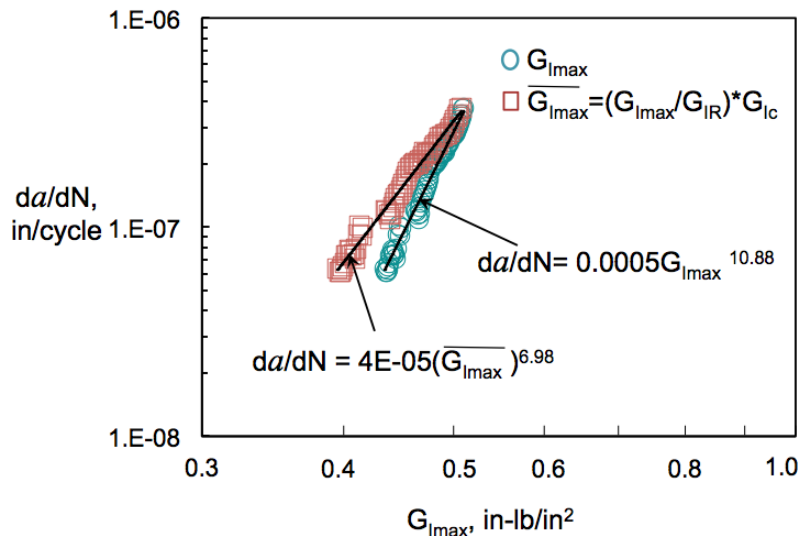


Figure 17. Normalized and non-normalized  $G_{I\max}$  for Source 1 specimen tested at 37% $G_{lc}$ .

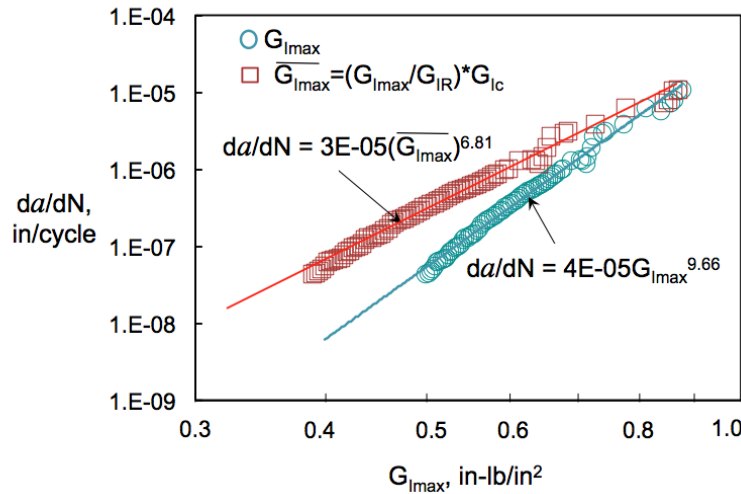


Figure 18. Normalized and non-normalized  $G_{I\max}$  for Source 2 specimen tested at 59% $G_{Ic}$ .

The technique of using an R-curve generated in static testing to account for fiber-bridging under fatigue loading is commonly used [6-7, 9-11]. However, the amount of fiber-bridging that actually occurs in fatigue is likely to be a function of the maximum opening displacement applied to the specimen. Therefore, the practice of correcting fatigue data generated at lower levels of  $G_{I\max}/G_{Ic}$  using an R-curve generated at much higher opening displacements may be overly conservative. However, the technique is still considered useful as a first approach to assess the contribution of fiber-bridging to delamination growth rate.

Figure 19 shows the normalized version of the results presented in Fig. 14 for Source 1. The Paris Law equation, shown on the figure, was fit to the combined data set. Comparing Figs. 14 and 19 shows that the slope of the data has decreased, as well as the spread of the data along the  $G_{I\max}$  axis, with the normalized data

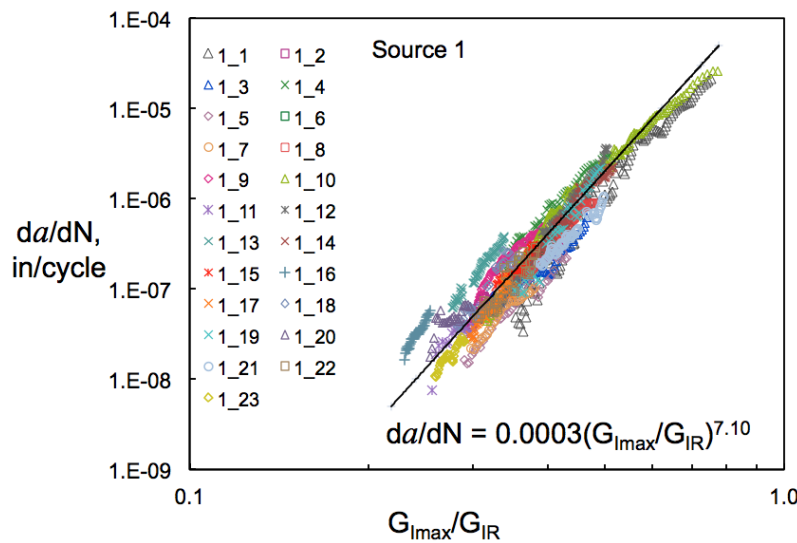


Figure 19. Normalized delamination growth results for Source 1. Paris Law equation is fit to combined data set.

forming a more unified set. Figure 20 shows the normalized version of Fig. 16 for the Source 2 specimens, with the Paris Law equation, fit to the combined data, also shown on the figure. As for the Source 1 specimens, the slope of the Paris Law and the range of the data are decreased in the normalized data set.

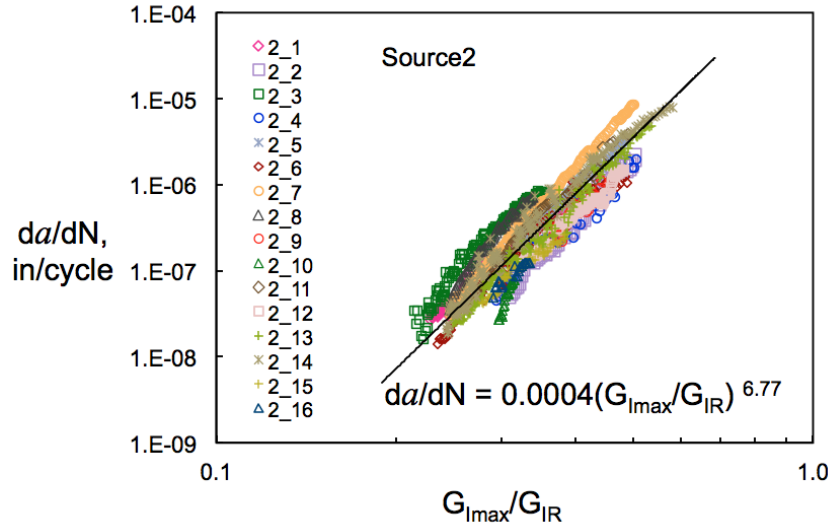


Figure 20. Normalized delamination growth results for Source 2 using MCC. Paris Law equation is fit to combined data set.

Figure 21 shows the normalized data from both sources plotted together. The slopes are similar for the two sources, but the two data sets do not completely overlap each other. These results are similar to those of ref. 12, where Paris Law expressions were generated for the mode II fatigue growth. Those Paris Laws also had similar exponents for Sources 1 and 2, but different constants, causing the Source 1 and Source 2 data sets to be offset slightly.

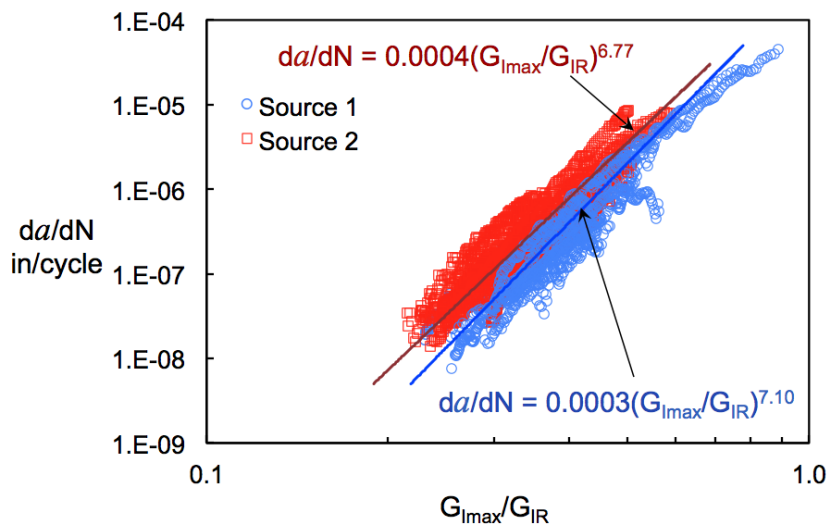


Figure 21. Normalized delamination growth results for Sources 1 and 2 using MCC.

Figures 22 and 23 show the Source 1 and 2 normalized data grouped by the initial  $G_{I\max}$  test level. Within each load level, the results were reasonably consistent for both sources; however, there was more scatter at lower load levels. This trend was observed in both sources, and may occur because at the lower load levels, as the delamination grows, the test machine is unable to maintain the load as consistently as at the higher levels. In both figures, there seems to be a tendency for the data to shift toward the left side of the data band as the  $G_{I\max}$  level decreases (orange triangles.) Figure 22 also shows results for two Source 1 specimens tested at approximately 28%  $G_{lc}$  for which delamination growth was observed. However, none of the Source 2 specimens tested below 30%  $G_{lc}$  delaminated.

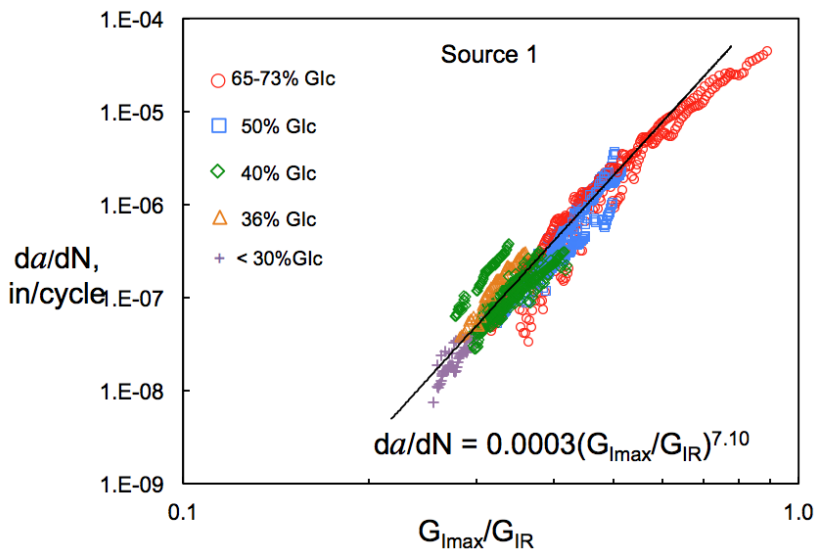


Figure 22. Normalized delamination growth results for Source 1 by initial  $G_{I\max}$  level.

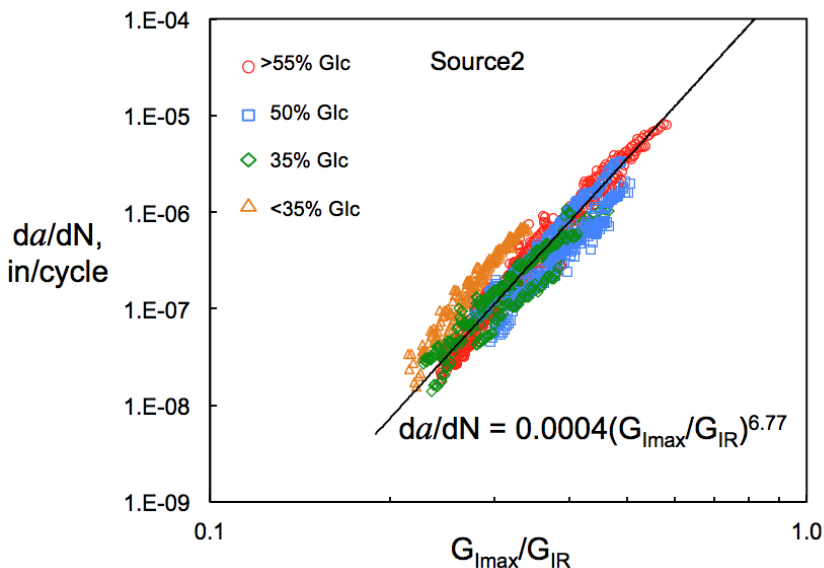


Figure 23. Normalized delamination growth results for Source 2 by initial  $G_{I\max}$  level.

### *Individual Compliance Calibration Fit*

The reliability of the fatigue results shown in Figs. 13-23 depends on the accuracy of the compliance calibration constants determined from the static tests. The compliance calibration constants in Table 1 were determined by a least squares fit to the combined static data, as shown in Figs. 5 and 6. When the constants are determined from each static specimen separately, the resulting slopes ( $A_1$  and  $m$ ) are similar to the combined value, differing by less than +/- 5%. However, the intercept values ( $k$  and  $|\Delta|$ ) can have significant differences. For the combined Source 1 static specimens, the value of  $k$  was -1.12, but for the individual specimens,  $k$  varied from -1.09 to -1.79, with a Coefficient of Variation (CoV) of 27%. For the combined Source 2 static specimens, the combined  $k$  value was -1.14, but values for the individual specimens ranged from -0.72 to -2.21 and the CoV was 62%. To attempt to determine the influence of using averaged static data on the resulting fatigue data and Paris Law, compliance calibration constants based on fatigue results were determined individually for some of the test specimens.

For every specimen for which there were adequate edge photos or visual recordings of the edge delamination length from the fatigue testing (approximately half of the specimens from each source), the visual data were used to generate a plot similar to Fig. 6. The compliance value corresponding to each observed delamination length was found from the raw fatigue data using the data record that related the number of loading cycles to the photo number. A minimum of 4 visual recordings was used for each specimen data fit, with the final recording usually taken at over 800K cycles. The individually fit values of  $A_1$  ranged from 61.0 to 76.8 for the Source 1 specimens and had an average value of 70.1, compared to the combined value of 68.8 from Table 1. The  $k$  values ranged from -0.01 to -2.49 with an average value of -1.22. For the Source 2 specimens,  $A_1$  ranged from 63.6 to 76.9 and had an average value of 70.0, compared to the combined value of 69.2. The  $k$  values for the Source 2 specimens ranged from -0.05 to -2.63 with an average value of -1.06. After determining  $A_1$  and  $k$  for each specimen, the  $da/dN$  vs.  $G_{I\max}/G_{IR}$  plots were recalculated.

Figure 24 shows the  $G_{I\max}$  results from Fig. 14 (using averaged static compliance parameters) for all the Source 1 specimens for which  $A_1$  and  $k$  could be fit. Figure 25 shows the results for the same specimens calculated using individually fit parameters. The correlation between the specimens is much improved over Fig. 24 and the slope of the Paris Law has increased. The corresponding data for Source 2 are shown in Figs. 26 and 27. Again, using the individually fitted compliance constants (Fig. 27) resulted in much better agreement of the different specimens. In this case the Paris Law exponent increased. Figures 28 and 29 show the normalized versions of Figs. 25 and 27. Both data sets now show very good alignment of the individual specimens and the resulting Paris Law expressions show good agreement.

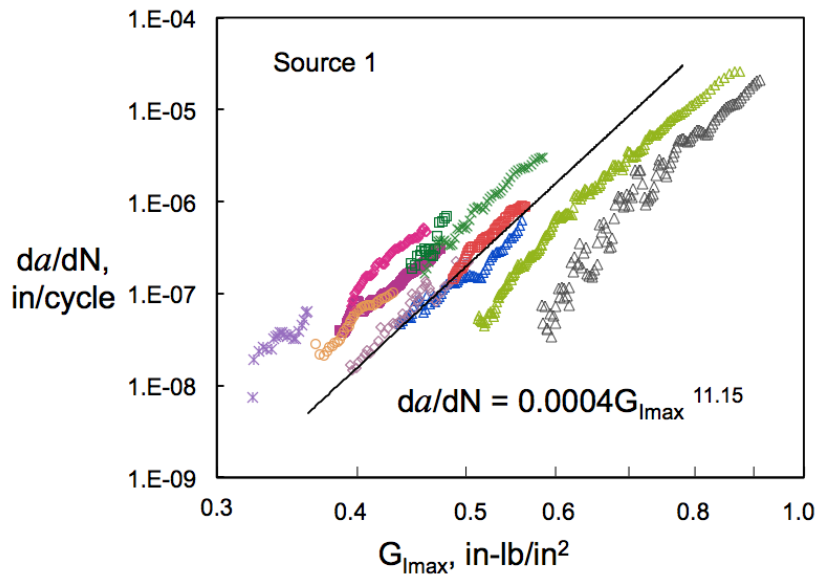


Figure 24. Delamination growth results for Source 1 using compliance calibration constants from static data.

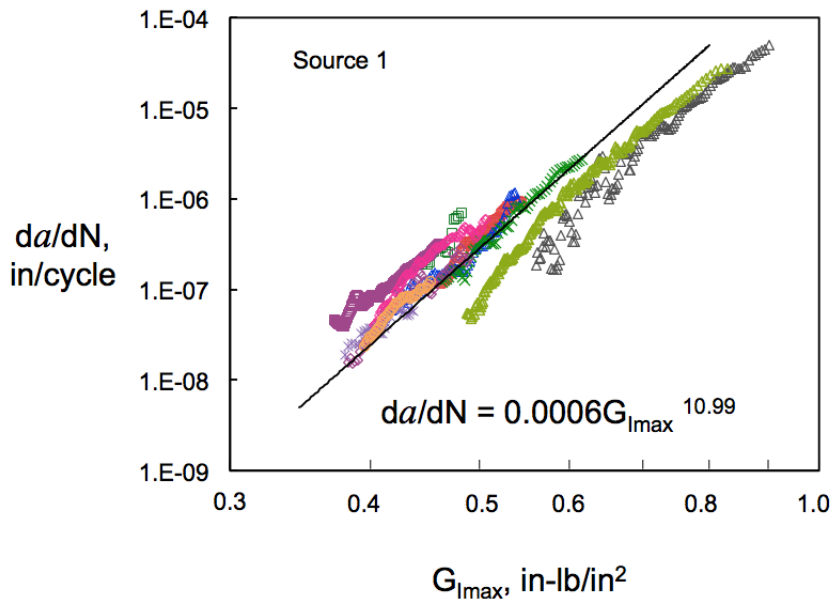


Figure 25. Delamination growth results for Source 1 using individually fit compliance calibration constants from fatigue data.

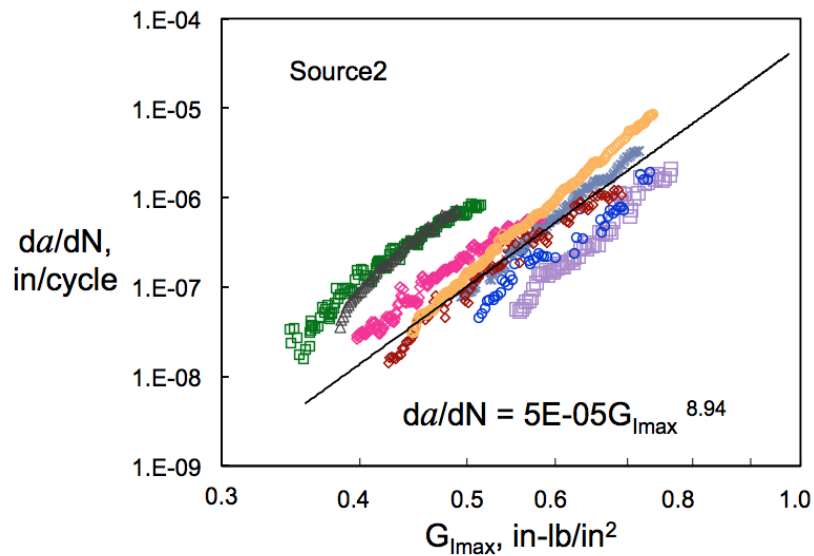


Figure 26. Delamination growth results for Source 2 using compliance calibration constants from static data.

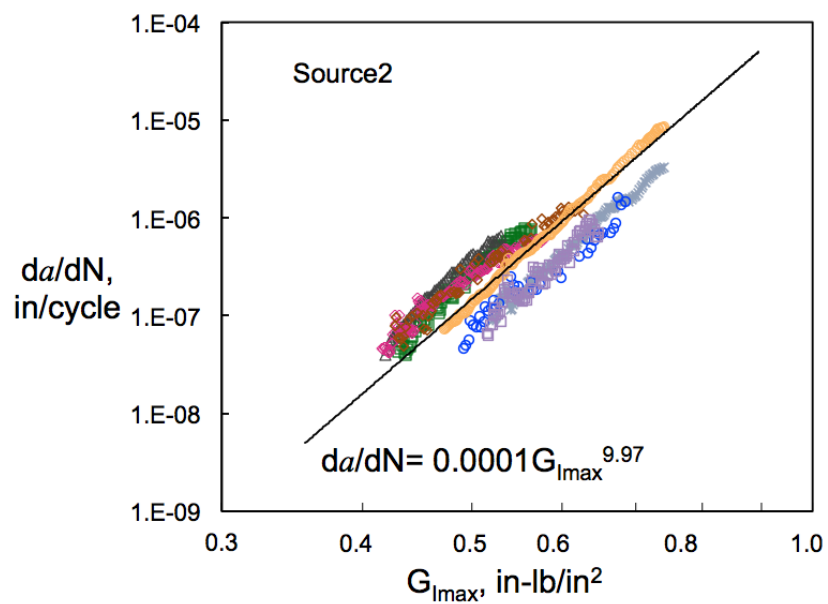


Figure 27. Delamination growth results for Source 2 using individually fit compliance calibration constants from fatigue data.

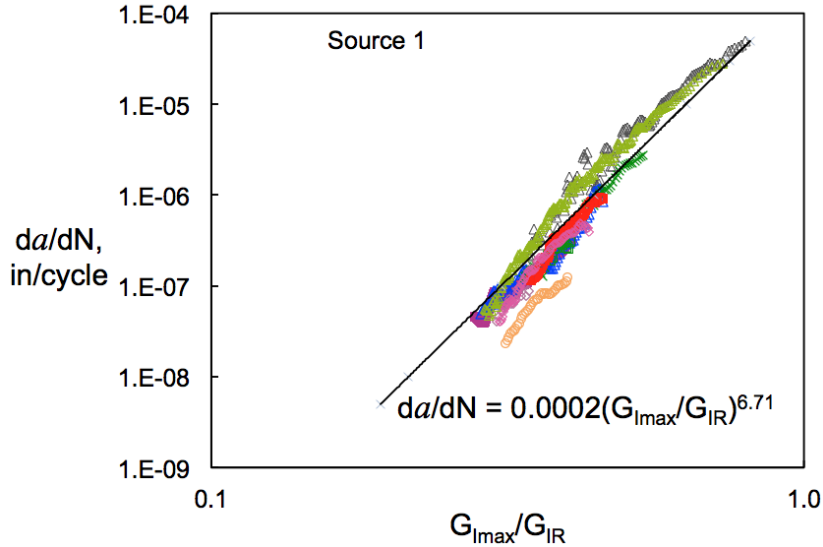


Figure 28. Normalized delamination growth results for Source 1 using individually fit compliance calibration constants from fatigue data.

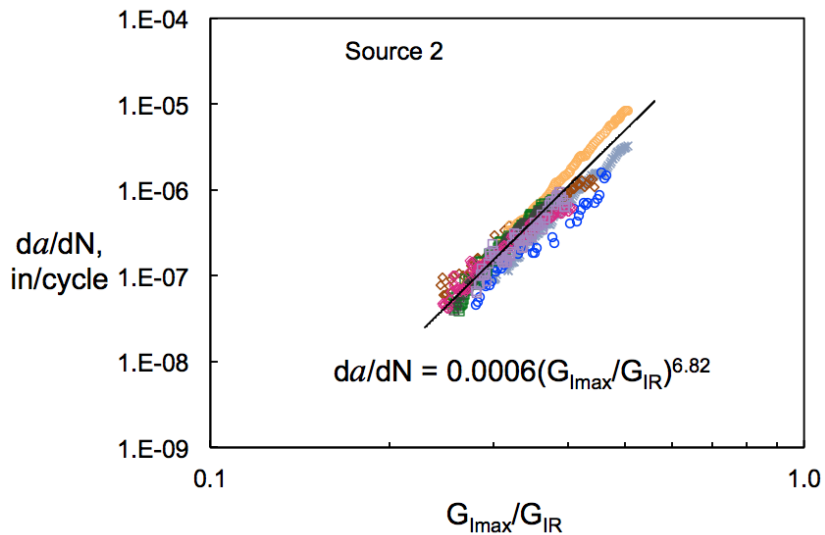


Figure 29. Normalized delamination growth results for Source 2 using individually fit compliance calibration constants from fatigue data.

## Summary

Double-cantilevered beam specimens of IM7/8552 manufactured by two sources were tested in static and fatigue to determine delamination characterization data for use in finite element modeling, and to compare the experimental results from the two different sources. Additionally, the fatigue tests were used to evaluate a proposed ASTM standard for determining Paris Law expressions for delamination growth under mode I loading. Strain energy release rates were calculated using

both the Modified Beam Theory (MBT) method and the Modified Compliance Calibration (MCC) method.

Static tests were conducted according to ASTM Standard D5528. The static tests were used to calculate fracture toughness, as well as compliance calibration constants and delamination resistance curves for use in the fatigue data reduction.

Fatigue DCB tests were conducted at initial  $G_{I\max}$  levels nominally equal to 50, 40 and 30%  $G_{Ic}$ , to generate a delamination onset threshold curve, and delamination growth data. Delamination onset curves were generated by plotting the initial  $G_{I\max}$  value versus the number of loading cycles to a 5% increase in compliance. Power law expressions were fit to the data plots.

To generate delamination growth data, each fatigue specimen was cycled until the delamination growth rate had decreased to at least  $1 \times 10^{-7}$  in/cycle, or until no delamination growth could be detected by at least  $1.5 \times 10^6$  cycles. The fatigue data were reduced according to the specifications of a proposed draft standard for delamination propagation. Both a 2-point secant method and a 7-point sliding-fit method were used to calculate the delamination growth rate,  $da/dN$ , for each fatigue specimen. In order to determine the effect of fiber-bridging on the  $da/dN$  results, the  $G_{I\max}$  values were normalized by the delamination resistance curves,  $G_{IR}$ , and replotted versus  $da/dN$ . Paris Law equations were fit to the normalized and non-normalized data sets for each source. Compliance calibration parameters were individually calculated for approximately half of the test specimens, using visual data recordings or photos taken during fatigue testing, and the  $G_{I\max}$  data was recalculated and compared to the results using averaged static parameters.

The following observations were made:

1. The averaged compliance calibration constants and the delamination resistance curves were very similar for the two sources and for the two data reduction methods. The  $G_{Ic}$  calculations from MBT and MCC were identical for each source; however, the Source 2 average fracture toughness was found to be approximately 13% higher than the Source 1 value.
2. The onset threshold curves for Sources 1 and 2 were similar, however, Source 2 specimens had longer lifetimes to delamination onset at every load level, compared to the Source 1 results.
3. The 7-point sliding-fit data reduction resulted in plots with reduced scatter compared to the 2-point method. The exponents of the Paris Law equations usually differed by 3% or less for the two methods; therefore, the 7-point method was considered accurate for calculating  $da/dN$  versus  $G_{I\max}$  data.
4. For each source, the slopes of the  $da/dN$  versus  $G_{I\max}$  plots were similar for the specimens tested, but the data sets were spread over a wide range of  $G_{I\max}$ . Results from the MCC method tended to be slightly more compact than from MBT, but neither method yielded a plot that was suitable for fitting a Paris Law to the combined data.
5. For both the Source 1 and Source 2 specimens, normalizing the  $G_{I\max}$  data by the  $G_{IR}$  curve resulted in a decrease in the Paris Law exponent of approximately 31 to 37%. Additionally, the normalized results reduced the spread of the results over  $G_{I\max}$  and resulted in a more compact data set.

- Using individually fit compliance parameters based on fatigue data from each specimen resulted in much better agreement between specimens at all  $G_{I\max}$  levels than results achieved using averaged parameters from the static data. The normalized  $G_I$  results showed excellent alignment of the specimens for both sources.

## References

- “ASTM D 5528-01, Standard Test Method for Mode I Interlaminar Fracture Toughness of Unidirectional Fiber-Reinforced Polymer Matrix Composites,” in *Annual Book of ASTM Standards*, Vol. 15.03, American Society for Testing and Materials, 2008.
- “ASTM D 6115-97, Standard Test Method for Mode I Fatigue Delamination Growth Onset of Unidirectional Fiber-Reinforced Polymer Matrix Composites,” in *Annual Book of ASTM Standards*, Vol. 15.03, American Society for Testing and Materials, 2008.
- “Standard Test Method for Mode I Fatigue Delamination Propagation of Unidirectional Fiber-Reinforced Polymer Matrix Composites,” Draft standard, ASTM International, Committee D30 on Composites, 2009.
- O’Brien, T. K., “Towards a Damage Tolerance Philosophy for Composite Materials and Structures,” *Composite Materials: Testing and Design (Ninth Volume)*, ASTM STP 1059, S. P. Garbo, Ed., American Society for Testing and Materials, Philadelphia, 1990, pp. 7-33.
- Martin, R. H., and Murri, G. B., “Characterization of Mode I and Mode II Delamination Growth and Thresholds in AS4/PEEK Composites,” *Composite Materials: Testing and Design (Ninth Volume)*, ASTM STP 1059, S. P. Garbo, Ed., American Society for Testing and Materials, Philadelphia, 1990, pp. 251-270.
- Shivakumar, K., Chen, H., and Abali, F., “A Total Fatigue Life Model for Mode I Loaded Composite Laminates,” *International Journal of Fatigue*, Vol. 28, Issue 1, January 2006, pp. 33-42.
- “Fatigue Fracture Toughness,” in *Composite Materials Handbook CMH-17*, Rev. G, Vol. 1, Section 6.9.4, SAE International, 2012.
- Johnson, W. S., and Mangalgiri, P. D., “Investigation of Fiber Bridging in Double Cantilever Beam Specimens,” *Journal of Composites Technology and Research*, Vol. 9, No. 1, Spring 1987, pp.10-13.
- Poursartip, A., “Characterization of Edge Delamination Growth in Laminates Under Fatigue Loading,” *Toughened Composites*, ASTM STP 937, Norman J. Johnston, Ed., American Society for Testing and Materials, Philadelphia, 1987, pp. 222-241.
- Giannis, S., Hansen, K., and Martin, R. H., “Accounting for the R-curve Effects on the Mode I Fatigue Delamination Growth Characterisation of Unidirectional Composites,” *Proceedings of the American Society for Composites*, Twenty-fifth Technical Conference, Dayton, Ohio, September 20-22, 2010.
- Murri, G. B., “Effect of Data Reduction and Fiber-Bridging on Mode I Delamination Characterization of Unidirectional Composites,” *Proceedings of the American Society for Composites*, 26th ASC Annual Technical Conference/2nd Joint US-Canada Conference on Composites, Montreal, Quebec, Canada, September 26-28, 2011.
- O’Brien, T. K., Johnston, W. M., and Toland, G. J., “Mode II Interlaminar Fracture Toughness and Fatigue Characterization of a Graphite Epoxy Composite Material,” NASA TM-2010-216838, August 2010.
- “ASTM D 5229/D 5229 M-92, Standard Test Method for Moisture Absorption Properties and Equilibrium Conditioning of Polymer Matrix Composite Materials,” in *Annual Book of ASTM Standards*, Vol. 15.03, American Society for Testing and Materials, 2008.
- Kaleidagraph, V4.1, Synergy Software, 2009.
- “ASTM E 647-00, Standard Test Method for Measurement of Fatigue Crack Growth Rates,” in *Annual Book of ASTM Standards*, Vol. 03.01, American Society for Testing and Materials, 2000.

REPORT DOCUMENTATION PAGE				Form Approved OMB No. 0704-0188	
<p>The public reporting burden for this collection of information is estimated to average 1 hour per response, including the time for reviewing instructions, searching existing data sources, gathering and maintaining the data needed, and completing and reviewing the collection of information. Send comments regarding this burden estimate or any other aspect of this collection of information, including suggestions for reducing this burden, to Department of Defense, Washington Headquarters Services, Directorate for Information Operations and Reports (0704-0188), 1215 Jefferson Davis Highway, Suite 1204, Arlington, VA 22202-4302. Respondents should be aware that notwithstanding any other provision of law, no person shall be subject to any penalty for failing to comply with a collection of information if it does not display a currently valid OMB control number.</p> <p><b>PLEASE DO NOT RETURN YOUR FORM TO THE ABOVE ADDRESS.</b></p>					
1. REPORT DATE (DD-MM-YYYY)	2. REPORT TYPE		3. DATES COVERED (From - To)		
01-02 - 2013	Technical Memorandum				
4. TITLE AND SUBTITLE			5a. CONTRACT NUMBER		
Evaluation of Delamination Onset and Growth Characterization Methods under Mode I Fatigue Loading			5b. GRANT NUMBER		
			5c. PROGRAM ELEMENT NUMBER		
6. AUTHOR(S)			5d. PROJECT NUMBER		
Murri, Gretchen B.			5e. TASK NUMBER		
			5f. WORK UNIT NUMBER		
			794072.02.07.03.03		
7. PERFORMING ORGANIZATION NAME(S) AND ADDRESS(ES)				8. PERFORMING ORGANIZATION REPORT NUMBER	
NASA Langley Research Center Hampton, VA 23681-2199				L-20229	
9. SPONSORING/MONITORING AGENCY NAME(S) AND ADDRESS(ES)				10. SPONSOR/MONITOR'S ACRONYM(S)	
National Aeronautics and Space Administration Washington, DC 20546-0001				NASA	
				11. SPONSOR/MONITOR'S REPORT NUMBER(S)	
				NASA/TM-2013-217966	
12. DISTRIBUTION/AVAILABILITY STATEMENT					
Unclassified - Unlimited					
Subject Category 24					
Availability: NASA CASI (443) 757-5802					
13. SUPPLEMENTARY NOTES					
14. ABSTRACT					
Double-cantilevered beam specimens of IM7/8552 graphite/epoxy from two different manufacturers were tested in static and fatigue to compare the material characterization data and to evaluate a proposed ASTM standard for generating Paris Law equations for delamination growth. Static results were used to generate compliance calibration constants for reducing the fatigue data, and a delamination resistance curve, GIR, for each material. Specimens were tested in fatigue at different initial cyclic GI <sub>max</sub> levels to determine a delamination onset curve and the delamination growth rate. The delamination onset curve equations were similar for the two sources. Delamination growth rate was calculated by plotting da/dN versus GI <sub>max</sub> on a log-log scale and fitting a Paris Law. Two different data reduction methods were used to calculate da/dN. To determine the effects of fiber-bridging, growth results were normalized by the delamination resistance curves. Paris Law exponents decreased by 31% to 37% after normalizing the data. Visual data records from the fatigue tests were used to calculate individual compliance constants from the fatigue data. The resulting da/dN versus GI <sub>max</sub> plots showed improved repeatability for each source, compared to using averaged static data. The Paris Law expressions for the two sources showed the closest agreement using the individually fit compliance data.					
15. SUBJECT TERMS					
Paris Law; composites; delamination; fatigue; fiber-bridging; strain energy release rate					
16. SECURITY CLASSIFICATION OF:			17. LIMITATION OF ABSTRACT	18. NUMBER OF PAGES	19a. NAME OF RESPONSIBLE PERSON
a. REPORT	b. ABSTRACT	c. THIS PAGE			STI Help Desk (email: help@sti.nasa.gov)
U	U	U	UU	32	19b. TELEPHONE NUMBER (Include area code) (443) 757-5802